CrossMark

Turbulent thermohaline hydraulic jumps

Raouf Emile Baddour†

Department of Civil & Environmental Engineering, University of Western Ontario, London, Ontario, N6A 5B9 Canada

Turbulent entrainment properties of thermohaline internal hydraulic jumps in quiescent ambient water are investigated. Underflow and overflow jumps are considered. The study is mainly concerned with thermohaline buoyancy effects on flow development. The thermohaline buoyancy is determined from a seawater equation of state, which is nonlinear in temperature and linear in salinity, and is accurate throughout the range of temperature and salinity of interest ($T = 0$ to $40\,°C$ and $S = 0$ to 40 ppt). The results indicate that thermohaline buoyancy produces smaller less diluted underflow jumps and larger more diluted overflow jumps. These nonlinear buoyancy effects are particularly significant when buoyancy arising from temperature and salinity act in opposite directions. Hydraulic controls by vertical and/or horizontal constrictions downstream reveal, using a matching technique, unique stationary miscible jump solutions.

Key words: hydraulics, stratified turbulence, hydraulic control

1. Introduction

Internal hydraulic jumps in stably stratified environments are observed in oceans, inland waters and the atmosphere. They occur in areas close to vertical and horizontal constrictions (Baines 1984, 1998). Internal hydraulic jumps in stably stratified environments can be traced back to studies by Long (1953, 1954), Benton (1954) and Yih and Guha (1955). Also, Armi (1986) and Lawrence (1993) conducted investigations on the hydraulics of two-layer flows and reviewed previous work in this field. Most internal jump investigations have assumed the pressure to remain hydrostatic and, generally, have ignored mixing across the interface.

Entrainment and mixing across density interfaces are relevant in geophysical and environmental applications. Among many natural and industrial thermohaline applications, the brilliant idea of Stommel and Farmer (1953) of controlling mixing in stratified fjords and channels has motivated this ongoing research. Furthermore, this work is related to internal hydraulic jumps observed in the ocean. An example is the

† Email address for correspondence: rbaddour@uwo.ca

well-documented internal hydraulic jump of the Strait of Gibraltar (Armi and Farmer 1988; Thorpe *et al*. 2018 and others). This narrow passage connects salty warm water from the Mediterranean Sea to less salty and cooler water from the Atlantic Ocean. In this ocean water exchange, the buoyancy arising from temperature and that from salinity are in opposite directions. And, as will be shown in this paper, such a condition can produce significant nonlinear buoyancy effects.

Wilkinson and Wood (1971) investigated the miscible behaviour of an internal jump. They carried out a stationary miscible jump analysis by applying a one-dimensional momentum equation. They introduced the concept of a density jump by considering entrainment of ambient fluid. Research on miscible internal jumps in two-layer systems has also been carried out by many researchers including Chu and Baddour (1977), Baddour and Abbink (1983), Wood and Simpson (1984), Baddour (1987), Holland *et al*. (2002), Hassid, Regev & Poreh (2007), Thorpe and Li (2014), Ogden and Helfrich (2016), Baines (2016) and others.

Baddour (1991) defined the thermal hydraulic jump as a jump where the density field is only a function of temperature. This function of temperature in water applications is nonlinear. However, a saline hydraulic jump is a jump where the density field is only a function of salinity, and therefore, the temperature is constant. The saline jump is equivalent to the density jump introduced by Wilkinson and Wood (1971) because the density is practically a linear function of salinity. For the more general case of a thermohaline jump considered here, the temperature and salinity can vary, and both contribute to the buoyancy field.

In water applications of internal hydraulic jumps, the density field has commonly been determined using a simplified linear water equation of state. The accuracy of this assumption was examined by Baddour (1991), where, under winter conditions, the nonlinearity of the equation of state had profound effects on the flow. In fact, the flow development in the jump region was significantly altered when the temperature of ambient water was between 0 and 15 °C.

This study considers miscible entraining thermohaline jumps. As mentioned above, temperature and salt are both possible contributors to the buoyancy. As clearly demonstrated by Dadonau, Partridge & Linden (2020), double diffusive effects in thermohaline jets are diminished, close to the source, as the Reynolds number is increased. It is assumed in this study that the Reynolds number is sufficiently large and double diffusion is not altering the flow dynamics in the jump region.

The flows under consideration are illustrated in figure 1, where internal jumps are created by highly turbulent (Reynolds number $Re_0 \gg 1$) and supercritical (Froude number $Fr_0 > 1$) discharge Q_0, of width b_0, depth h_0, temperature T_0 and salinity S_0. The flow occurs either at the free surface (see overflow in figure 1a) or along the bottom (see underflow in figure 1b). The deep receiving ambient water has a temperature T_a, salinity S_a and a width $b_1 \geq b_0$. The temperature and salinity are such that the flow is stably stratified throughout the region of interest. Note, because of nonlinear thermohaline buoyancy, a turbulent flow, which is initially stably stratified, is not necessarily stably stratified after mixing (Turner 1966). Thermohaline jumps exhibiting reversible buoyancy arising from entrainment are not considered in this paper.

The entraining thermohaline jump is a rapidly varying phenomenon associated with changes in velocity, temperature, salinity and depth. Similar to a single-layer open channel flow, the internal jump is a transition from a supercritical flow ($Fr_0 > 1$) to a subcritical flow ($Fr_1 < 1$) (Henderson 1966). Owing to the entrainment of ambient fluid, the discharge (or flow rate) increases in the jump region from Q_0 to Q_1, the temperature
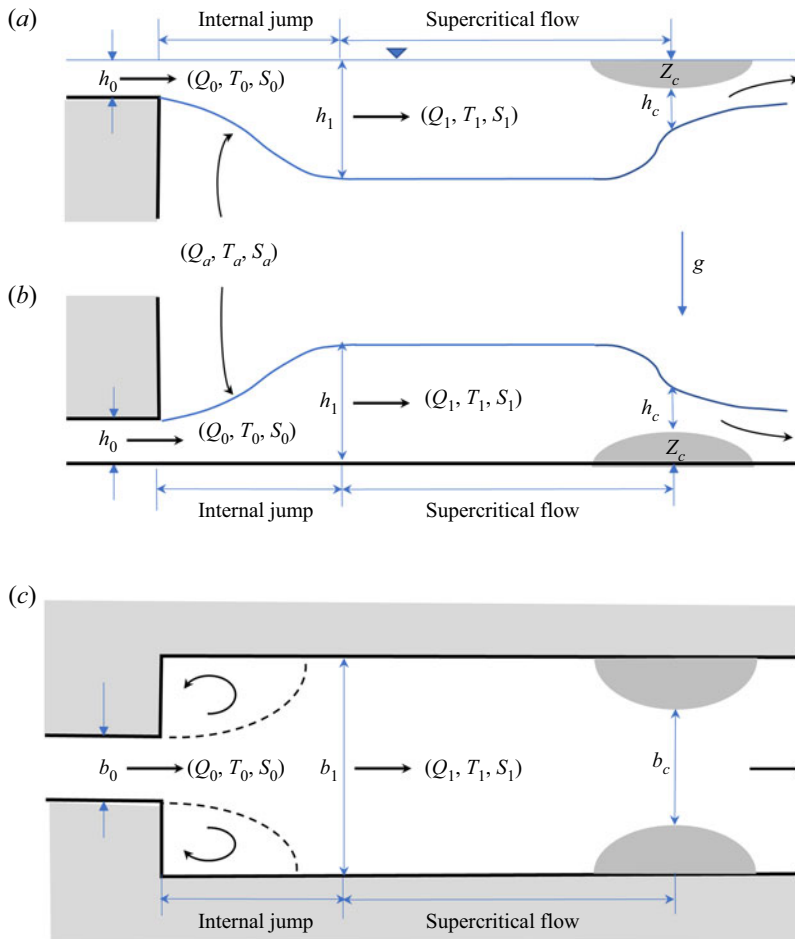
Figure 1. Definition sketches of stationary entraining thermohaline jumps upstream of vertical and horizontal constrictions, showing (*a*) side-view of overflow, (*b*) side-view of underflow and (*c*) top-view of overflow and underflow.

changes from T_0 to T_1 and salinity from S_0 to S_1. The depth of the mixed layer downstream of the jump is h_1 and its width is b_1. Two horizontal eddies are observed when the jump is three-dimensional ($b_1 > b_0$). The temperature and salinity in these horizontal eddies, which are attached to the upstream wall, are T_e and S_e. The laboratory experiment by Guo (1992) indicated that $T_e \approx T_1$ and $S_e \approx S_1$. Further downstream of the jump, vertical and/or horizontal constrictions of height Z_c and width b_c provide hydraulic controls, through which the flow is critical ($Fr_c = 1$).

Thermohaline buoyancy will first be derived in § 2, based on a seawater equation of state, which is nonlinear in temperature and linear in salinity. The thermohaline buoyancy will then be applied in § 3 to the conservation equations of temperature, salt and momentum. These simple basic equations reveal the nonlinear mixing behaviour of thermohaline jumps. Although, the miscible jump solutions obtained are not unique, they are clearly defining maximum entraining conditions, which are of practical interest. A matching technique will be used in § 4 to examine how downstream boundary conditions by vertical and/or horizontal constrictions determine unique jump solutions. Finally, in

§ 5, the internal jump theory will be compared with the two-dimensional (2-D) and three-dimensional (3-D) experiments by Guo (1992).

2. Thermohaline buoyancy

The international equation of state for seawater (Millero and Poisson 1981), which has a temperature T (°C) and salinity S (ppt or g kg^{-1}) is shown in figure 2. This equation is nonlinear throughout the range of temperature and salinity of interest ($T = 0$–40 °C and $S = 0$–40 ppt), and for all practical purposes can be expressed as

$$\rho(T, S) = f_1(T) + f_2(T)S, \qquad (2.1)$$

where ρ is the density of water in kg m^{-3}, and f_1 and f_2 are nonlinear functions of temperature. The function f_1 represents the density of pure fresh water, as determined by Bigg (1967). The function f_2 was determined in this study by fitting the salinity term of (2.1) to the salinity terms of the international equation of state for seawater by Millero and Poisson (1981). With f_1 and f_2 expressed as polynomials, the equation of state for seawater becomes

$$\rho(T, S) = \sum_{i=0}^{n} a_i T^i + S \sum_{i=0}^{m} b_i T^i. \qquad (2.2)$$

A linearized equation of state, which has been widely adopted for ocean and inland water modelling is (Whitehead 1995)

$$\rho(T, S) = \rho_0 + \alpha T + \beta S, \qquad (2.3)$$

where ρ_0 is a reference density, α a negative thermal expansion coefficient and β a positive saline contraction coefficient. It will be shown that such linear simplification is not always adequate. Brydon, Sun & Bleck (1999) and Nycander, Hieronymus & Roquet (2015) and others have also emphasized the need to apply a nonlinear equation of state for ocean modelling.

The degrees of the polynomials in (2.2) required to obtain accurate densities throughout the range of temperature and salinity of interest are $n = 5$ and $m = 2$. The constants of these two polynomials are (Baddour 1994) $a_0 = 999.842594$, $a_1 = 6.793952 \times 10^{-2}$, $a_2 = -9.095290 \times 10^{-3}$, $a_3 = 1.001685 \times 10^{-4}$, $a_4 = -1.120083 \times 10^{-6}$, $a_5 = 6.536332 \times 10^{-9}$, $b_0 = 0.806924$, $b_1 = -3.042878 \times 10^{-3}$ and $b_2 = 3.280458 \times 10^{-5}$. Densities calculated with (2.2) and the international equation of state at standard atmospheric pressure by Millero and Poisson (1981) are practically identical, with differences not exceeding 0.08 % throughout the range of temperature and salinity of interest. Millero (2010) provided an interesting historical account of the international seawater equation of state.

Density anomalies, and related buoyancy, were obtained in this study by transforming the coordinate system of (2.2) from (T, S, ρ) to $(\Delta T, \Delta S, \Delta \rho)$, where Δ represents an excess quantity relative to the ambient state (i.e. $\Delta T = T - T_a$, $\Delta S = S - S_a$ and $\Delta \rho = \rho - \rho_a$) and suffix a refers to the state of ambient water. This transformation was achieved, as illustrated in figure 3, by moving the origin of the frame of reference from (0,0,0) to (T_a, S_a, ρ_a). Note the new origin at (T_a, S_a, ρ_a) lies on the equation of state surface (see figure 3).
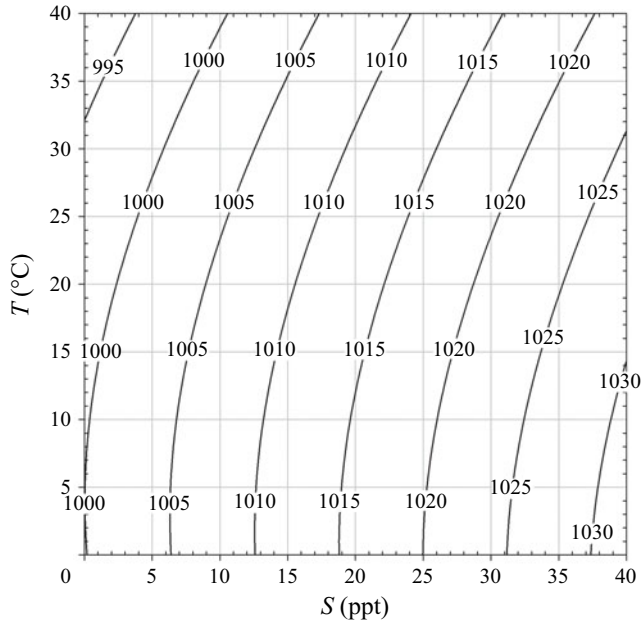
930 A5-4

Figure 2. Contour lines of seawater density ρ (kg m^{-3}) as a function of temperature T (°C) and salinity S (ppt) in the range of temperature (0–40 °C) and salinity (0–40 ppt).
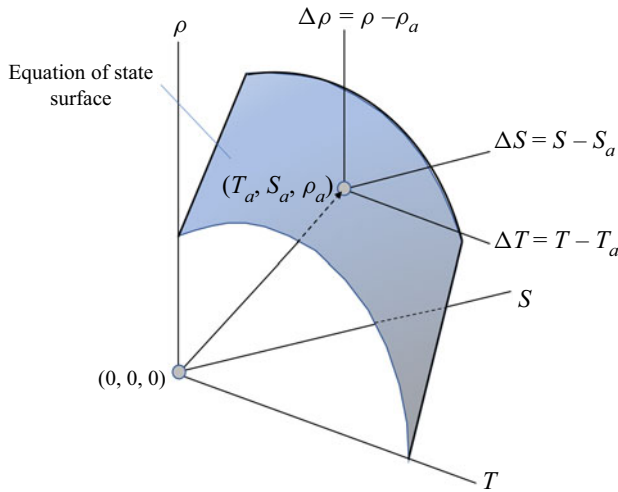

Figure 3. Transformation of the equation of state obtained by moving the origin of the frame reference from (0,0,0) to (T_a, S_a, ρ_a).

The polynomial transformation, defined above, gives the following expression for the density anomaly:

$$\Delta\rho = \sum_{i=1}^{n} a_i \Delta T^i + S_a \left(\sum_{i=1}^{m} \beta_i \Delta T^i \right) + \Delta S \left(\beta_0 + \sum_{i=1}^{m} \beta_i \Delta T^i \right), \qquad (2.4)$$

where

$$\alpha_i = \sum_{j=i}^{n} \binom{j}{i} a_j T_a^{j-i}; \quad i = 1, n, \tag{2.4a}$$

$$\binom{j}{i} = \frac{j!}{i!(j-i)!}, \tag{2.4b}$$

$$\beta_0 = \sum_{j=0}^{m} b_j T_a^j, \tag{2.4c}$$

$$\beta_i = \sum_{j=i}^{m} \binom{j}{i} b_j T_a^{j-i}; \quad i = 1, m. \tag{2.4d}$$

For $n = 5$, the coefficients α_i are

$$\left.\begin{aligned}
\alpha_1 &= a_1 + 2a_2 T_a + 3a_3 T_a^2 + 4a_4 T_a^3 + 5a_5 T_a^4 \\
\alpha_2 &= a_2 + 3a_3 T_a + 6a_4 T_a^2 + 10a_5 T_a^3 \\
\alpha_3 &= a_3 + 4a_4 T_a + 10a_5 T_a^2 \\
\alpha_4 &= a_4 + 5a_5 T_a \\
\alpha_5 &= a_5
\end{aligned}\right\}, \tag{2.5}$$

and for $m = 2$, the coefficients β_i are

$$\left.\begin{aligned}
\beta_0 &= b_0 + b_1 T_a + b_2 T_a^2 \\
\beta_1 &= b_1 + 2b_2 T_a \\
\beta_2 &= b_2
\end{aligned}\right\}. \tag{2.6}$$

A positive value of $\Delta\rho$ indicates an excess density compared to the ambient state (downward buoyancy), and a negative $\Delta\rho$ is a density deficit (i.e. upward buoyancy). Equation (2.4) is shown in figure 4 for a state of ambient water given by $T_a = 20\,°C$ and $S_a = 30$ ppt. This transformation is defining the positive and negative buoyancy regimes for any combinations of temperature difference $\Delta T = T - T_a$ and salinity difference $\Delta S = S - S_a$. Equation (2.4), which is plotted in figure 4, will be applied in the following section to determine the buoyancy associated with temperature and salinity differences in thermohaline jumps.

3. Thermohaline internal hydraulic jumps

3.1. *Governing equations*

The basic assumptions in the following analysis are: (i) discharge and ambient water conditions are steady; (ii) velocity, temperature and salinity profiles are uniform at the exit and downstream of the jump; (iii) density difference is everywhere relatively small ($\Delta\rho/\rho_a \ll 1$), which allows for the Boussinesq's approximation to be applied; (iv) discharge Reynolds number is high, which produces strong mixing with minimal manifestation of double diffusion; (v) the water in the horizontal eddies attached to the vertical upstream wall of three-dimensional jumps has temperature and salinity similar to the mixed water downstream of the jump, and (vi) heat and salt are conserved.
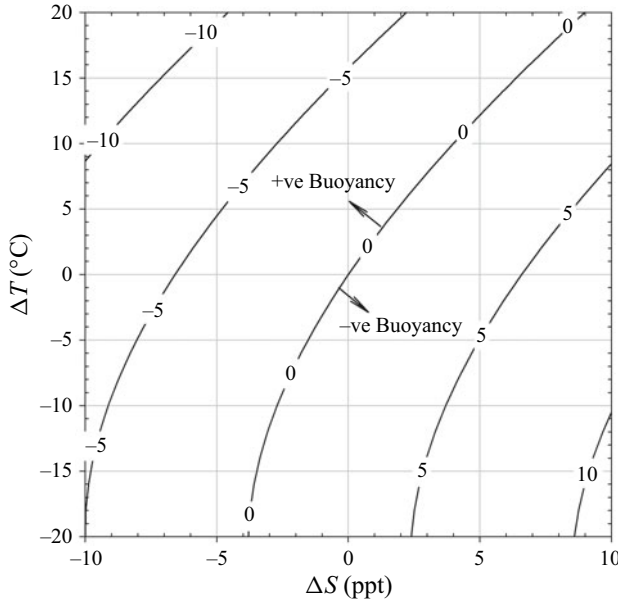
Figure 4. Density anomaly $\Delta\rho = \rho - \rho_a$ (kg m^{-3}) calculated with (2.4) as a function of temperature difference $\Delta T = T - T_a$ (°C) and salinity difference $\Delta S = S - S_a$ (ppt) for ambient water conditions $T_a = 20$ °C and $S_a = 30$ ppt.

Based on these assumptions, the governing equations for the temperature, salt and momentum of a stationary internal jump are

$$Q_0 \Delta T_0 = Q_1 \Delta T_1, \tag{3.1}$$

$$Q_0 \Delta S_0 = Q_1 \Delta S_1, \tag{3.2}$$

$$\frac{Q_1^2}{b_1 h_1} - \frac{Q_0^2}{b_0 h_0} = \frac{1}{2} g_0' h_0^2 b_0 + \frac{1}{2} g_1' [(h_0^2 (b_1 - b_0) - h_1^2 b_1)]. \tag{3.3}$$

In all the equations, subscript 0 refers to the supercritical flow upstream of the jump and subscript 1 to the subcritical flow downstream of the jump. The magnitude of the initial buoyancy (or effective gravity) upstream is $g_0' = g|\Delta\rho_0|/\rho_a$ and downstream is $g_1' = g|\Delta\rho_1|/\rho_a$, and g is the constant gravity.

The left-hand side of (3.3) represents the net flux of momentum in the jump region and the right-hand side of (3.3) represents the net hydrostatic force, which includes a component exerted by the upstream wall of width $(b_1 - b_0)$.

In addition to the above governing equations, it is important to recognize that the jump solutions cannot physically be associated with a gain of energy. This condition requires the total energy head of the flow downstream of the jump to be less than upstream of the jump. When the velocity profiles are uniform upstream and downstream of the jump, the total energy head is given by (Henderson 1966)

$$H = h + \frac{U^2}{2g'}, \tag{3.4}$$

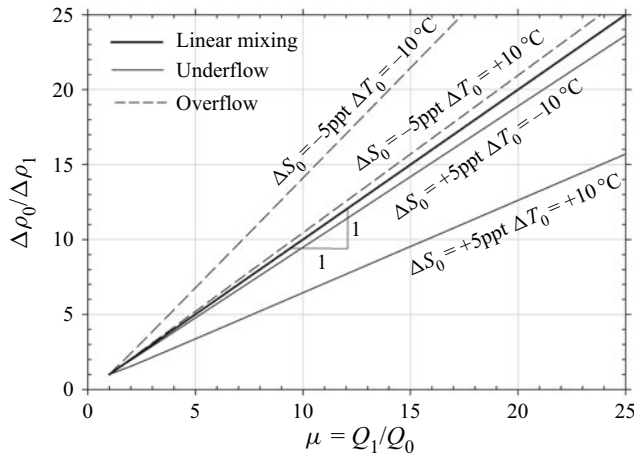and $U = Q/(bh)$ is a cross-sectional average velocity.

Figure 5. Comparison of linear and nonlinear mixing behaviour for thermohaline underflow and overflow jumps.

Hence, the energy constraint on the jump solution is

$$\left(h_1 + \frac{U_1^2}{2g'_1}\right) < \left(h_0 + \frac{U_0^2}{2g'_0}\right). \tag{3.5}$$

3.2. *Nonlinear thermohaline mixing*

Dilution resulting from ambient water entrainment into the jump is directly related to the ratio of discharge downstream and upstream of the jump. Hence, from (3.1) and (3.2), we can define the dilution in the jump as

$$\mu = \frac{Q_1}{Q_0} = \frac{\Delta T_0}{\Delta T_1} = \frac{\Delta S_0}{\Delta S_1}. \tag{3.6}$$

The effect of dilution (or mixing) on thermohaline buoyancy was first examined using (2.4) and (3.6). For a given dilution μ and initial values ΔT_0 and ΔS_0, (3.6) gives the excess temperature ΔT_1 and excess salinity ΔS_1 of the mixed fluid downstream of the jump. These properties of the mixed fluid are then translated into excess density $\Delta \rho_1$ using (2.4). Results obtained in this manner are plotted in figure 5 and compared with the mixing behaviour based on the linearized equation of state (2.3).

The density anomaly ratio $\Delta \rho_0 / \Delta \rho_1$ for a linear equation of state, is simply

$$\frac{\Delta \rho_0}{\Delta \rho_1} = \frac{\alpha \Delta T_0 + \beta \Delta S_0}{\alpha \Delta T_1 + \beta \Delta S_1} = \frac{\alpha \Delta T_0 + \beta \Delta S_0}{\alpha \frac{\Delta T_0}{\mu} + \beta \frac{\Delta S_0}{\mu}} = \mu. \tag{3.7}$$

This linear mixing behaviour is represented in figure 5 by the 1:1 slope line.

As illustrated in figure 6, the nonlinearity and concave downward curvature of the equation of state are responsible for producing density ratios $\Delta \rho_o / \Delta \rho_1 > \mu$ for overflows and $\Delta \rho_o / \Delta \rho_1 < \mu$ for underflows.

3.3. *Non-dimensional governing equations*

To generalize the results, the momentum equation (3.3) and the energy equation (3.5) are first expressed in non-dimensional forms as
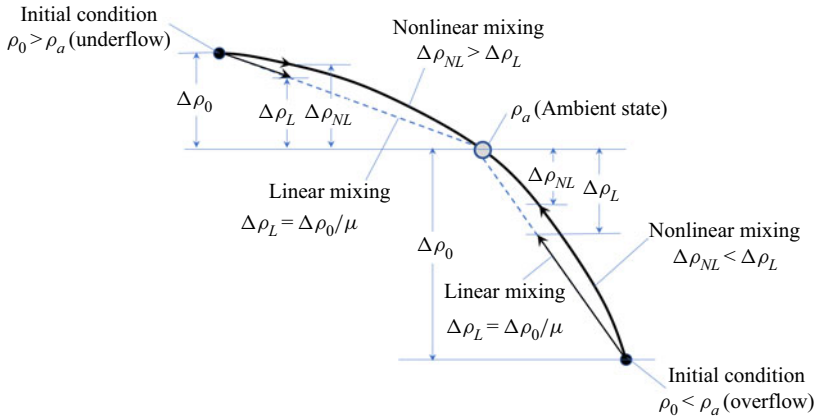
930 A5-8

Figure 6. Schematic illustration of linear and nonlinear (concave downward) mixing behaviour for underflows and overflows.

Momentum Equation:

$$Fr_0^2 = \frac{1}{2}\left(\frac{\beta r}{\mu^2 - \beta r}\right)\left(1 - \left(\frac{g'_1}{g'_0}\right)[\beta(r^2 - 1) + 1]\right). \tag{3.8}$$

Energy Equation:

$$\left[r + \frac{1}{2}\left(\frac{Fr_0^2}{\beta^2}\right)\left(\frac{\mu^2}{r^2}\right)\left(\frac{g'_0}{g'_1}\right)\right] < \left[1 + \frac{1}{2}Fr_0^2\right]. \tag{3.9}$$

Here, the discharge Froude number $Fr_0 = Q_0/\sqrt{(g'_0 b_0^2 h_0^3)}$, the depth ratio across the jump $r = h_1/h_0$ and the jump enlargement ratio $\beta = b_1/b_0$. Note, because of nonlinear mixing, the buoyancy flux across the jump is not conserved. In other words, $g'_0 Q_0 \neq g'_1 Q_1$ and therefore the dilution $\mu = Q_1/Q_0 \neq g'_0/g'_1$. The buoyancy flux for linear mixing is, of course, conserved because $\mu = \Delta\rho_0/\Delta\rho_1 = g'_0/g'_1$, and (3.8) reduces to

$$Fr_0^2 = \frac{1}{2}\left(\frac{\beta r}{\mu^2 - \beta r}\right)\left(1 - \frac{\beta(r^2 - 1) + 1}{\mu}\right). \tag{3.10}$$

For a 2-D flow $b_1 = b_0$, hence $\beta = 1$ and

$$Fr_0^2 = \frac{1}{2}\left(\frac{r}{\mu^2 - r}\right)\left(1 - \frac{r^2}{\mu}\right), \tag{3.11}$$

from which the classical hydraulic jump equation is correctly recovered by setting the dilution $\mu = 1$ (Rouse 1946):

$$Fr_0^2 = \tfrac{1}{2}r(1 + r). \tag{3.12}$$

And the only positive subcritical solution, shown in figure 7, of this quadratic equation is the well-known hydraulics formula:

$$r^* = \tfrac{1}{2}(\sqrt{1 + 8Fr_0^2} - 1). \tag{3.12a}$$

The dilution properties of internal hydraulic jumps were next examined by plotting the general (3.8) as $r = f(\mu)$, by setting both the discharge Froude number Fr_0 and channel
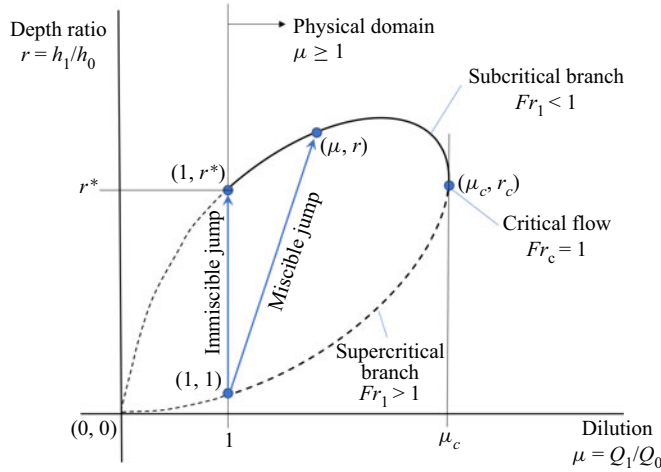
Figure 7. Dilution diagram of internal hydraulic jumps in deep and quiescent ambient water according to the momentum equation (3.8) and for $Fr_0 = \text{const.}$ and $\beta = \text{const.}$

enlargement ration β to be constants. These plots were obtained with an exact algorithm for determining all the real and imaginary roots of a cubic equation. The jump immiscible ($\mu = 1$) and miscible ($\mu > 1$) solutions are illustrated in figure 7. For the quiescent and deep ambient water condition, the miscible jump solutions always form closed loops in the μ–r plane. The loops are connected to the origin ($r = 0$, $\mu = 0$) and the size of the loop increases vertically with Fr_0 and horizontally with β. The upper branch (solid line in figure 7) of a loop is subcritical ($Fr_1 = Q_1/\sqrt{(g'_1 b_1^2 h_1^3)} < 1$) and the lower branch is supercritical ($Fr_1 > 1$). The subcritical and supercritical branches meet at the origin (0,0) as well as at a point where the flow is critical ($Fr_c = 1$) and where the dilution is reaching a maximum value μ_c.

The maximum possible dilution occurring in a channel is of practical interest. Differentiating (3.10) and setting $\mathrm{d}\mu/\mathrm{d}r = 0$, the maximum dilution for linear mixing is

$$\mu_c = \tfrac{1}{3} Fr_0^{-4/3} \beta^{1/3} (1 + 2Fr_0^2) \tag{3.13}$$

$$\approx \tfrac{2}{3} Fr_0^{2/3} \beta^{1/3} \quad \text{for } Fr_0 \gg 1, \tag{3.13a}$$

and the critical depth is

$$r_c = \tfrac{1}{3} Fr_0^{-2/3} \beta^{-1/3} (1 + 2Fr_0^2) \tag{3.14}$$

$$\approx \tfrac{2}{3} Fr_0^{4/3} \beta^{-1/3} \quad \text{for } Fr_0 \gg 1. \tag{3.14a}$$

Similar results for nonlinear mixing are obtained numerically using (3.8). Figure 8 shows results from (3.8) in the physical domain ($r \geq 0$, $\mu \geq 1$) for thermohaline jumps under linear and nonlinear mixing conditions. Effects of nonlinear mixing on maximum dilution μ_c are also presented in figure 9. It is evident from both figures 8 and 9 that nonlinear mixing increases the dilution and depth of thermohaline overflow jumps and decreases the dilution and depth of thermohaline underflow jumps. The results also indicate that nonlinear mixing effects are more significant when buoyancy arising from temperature and that from salinity are acting in opposite directions.

930 A5-10
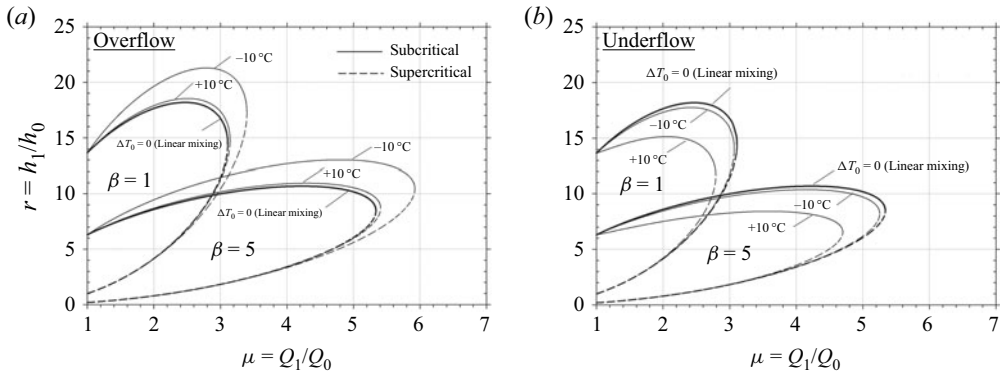
Figure 8. Dilution properties of stationary entraining thermohaline jumps obtained with (3.8), $Fr_0 = 10$, $T_a = 20\,°C$ and $S_a = 30$ ppt: (*a*) overflow, $\Delta S_0 = -5$ ppt; and (*b*) underflow, $\Delta S_0 = +5$ ppt.
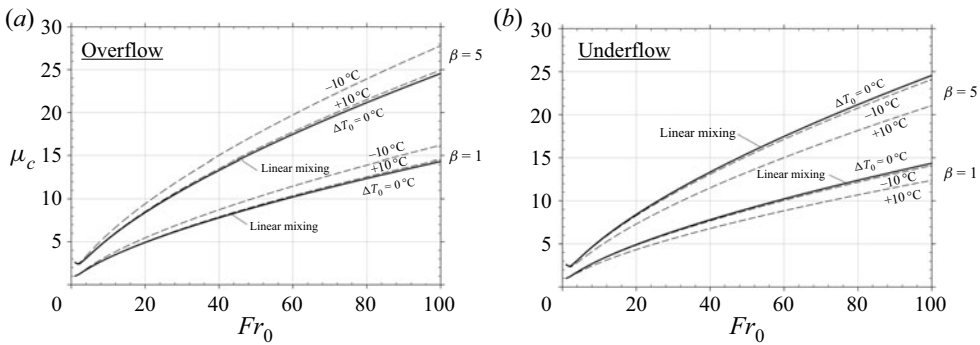

Figure 9. Maximum dilution of stationary entraining thermohaline jumps obtained with (3.8), $T_a = 20\,°C$, $S_a = 30$ ppt: (*a*) overflow, $\Delta S_0 = -5$ ppt; and (*b*) underflow, $\Delta S_0 = +5$ ppt.
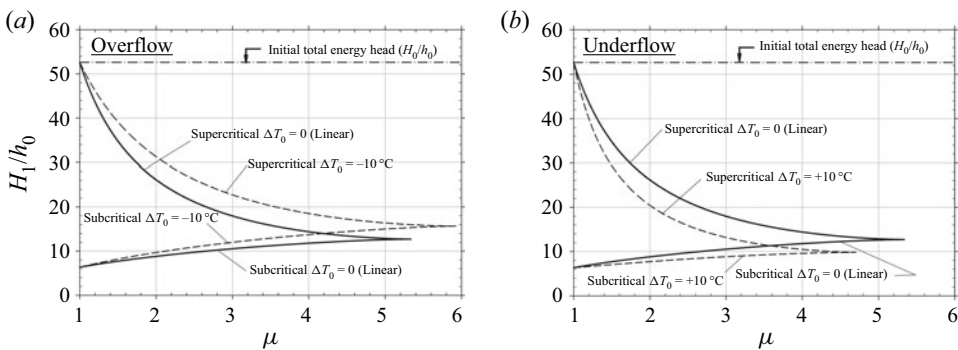

Figure 10. Total energy head of thermohaline jumps obtained with (3.8) and (3.9), $Fr_0 = 10$, $\beta = 5$, $T_a = 20\,°C$ and $S_a = 30$ ppt: (*a*) overflow, $\Delta S_0 = -5$ ppt; and (*b*) underflow, $\Delta S_0 = +5$ ppt.

3.4. *Energy considerations*

Energy constraints on miscible jumps given by (3.9) are examined in figure 10. Total energy heads for overflow jumps are plotted in figure 10(*a*) for linear and nonlinear mixing conditions. Similar results for underflow jumps are presented in figure 10(*b*). Figure 10(*a*)

930 A5-11

shows that nonlinear mixing systematically increases the total head of the supercritical and subcritical branches of the overflow jump. The opposite effect can be seen in figure 10(*b*), where nonlinear mixing decreases the total head of the underflow jump. Consistent with the results obtained from the momentum equation, the nonlinearity effects on the total energy head were more pronounced when the buoyancy arising from temperature and that from salinity were acting in opposite directions. Furthermore, the total head H/h_0 of the supercritical branches were always smaller than the initial total head H_0/h_0, but always higher than the total head of the subcritical branches. This observation indicates, on energetic grounds, that the miscible entraining thermohaline jump is a physically possible transition from supercritical to subcritical flow, and not vice versa.

4. Downstream hydraulic control

Effects of downstream boundary conditions on the miscible jump solutions obtained in § 3 are analysed here. The assumptions of this analysis are: (i) there is no entrainment of ambient water in the subcritical region downstream of the jump; (ii) there is no loss of energy in the short distance separating the jump from the channel end; (iii) a hydraulic control is established at the section of maximum vertical and/or horizontal contraction, where flow reaches a critical state in a manner similar to single-layer open channel hydraulics (Henderson 1966).

For a maximum height of sill Z_c, which coincides with a minimum channel width b_c, the critical flow condition is $Fr_c^2 = Q_1^2/g_1' b_c^2 h_c^3 = 1$ and the critical depth $h_c = (Q_1^2/g_1' b_c^2)^{1/3}$ (Henderson 1966).

Because there is no entrainment downstream of the jump, the discharge remains constant and $Q_c = Q_1$. Similarly, the density does not change downstream of the jump and $g_c' = g_1'$.

Furthermore, conserving energy of the subcritical flow through the sill and/or contraction requires the total head $H_1 = Z_c + H_c$. Additionally, from basic hydraulics of rectangular channels, the critical head $H_c = \frac{3}{2}h_c$ (Henderson 1966). Hence, the downstream boundary condition applied to the jump can finally be written as

$$h_1 + \frac{Q_1^2}{2g_1' b_1^2 h_1^2} = Z_c + \frac{3}{2}\left(\frac{Q_1^2}{b_c^2 g_1'}\right)^{1/3}, \tag{4.1}$$

and in non-dimensional form, the downstream boundary condition is

$$r + \frac{1}{2}\left(\frac{Fr_0}{\beta}\right)^2 \left(\frac{\mu}{r}\right)^2 \left(\frac{g_0'}{g_1'}\right) = \lambda_c + \frac{3}{2}\left(\frac{Fr_0}{\beta_c}\right)^{2/3} \mu^{2/3} \left(\frac{g_0'}{g_1'}\right)^{1/3}, \tag{4.2}$$

where $\beta_c = b_c/b_0$ and $\lambda_c = Z_c/h_0$.

Note, the linear mixing approximation of (4.2) (case of $g_0'/g_1' = \mu$) is

$$1 + \frac{1}{2}\left(\frac{Fr_0}{\beta}\right)^2 \left(\frac{\mu}{r}\right)^3 = \frac{\lambda_c}{r} + \frac{3}{2}\left(\frac{Fr_0}{\beta_c}\right)^{2/3}\left(\frac{\mu}{r}\right). \tag{4.3}$$

Subcritical branches of the general (4.2), plotted as $\mu = f(r)$, are superimposed in figure 11 on the momentum equation (3.8), which was formulated in § 3.

The jump solutions are required to satisfy simultaneously the momentum equation (3.8) and the hydraulic control (4.2). The solutions in the $\mu - r$ plane are, therefore, the points of intersection of (3.8) and (4.2). This matching technique is applied in figure 11 to determine the solutions associated with specified discharge and downstream conditions.
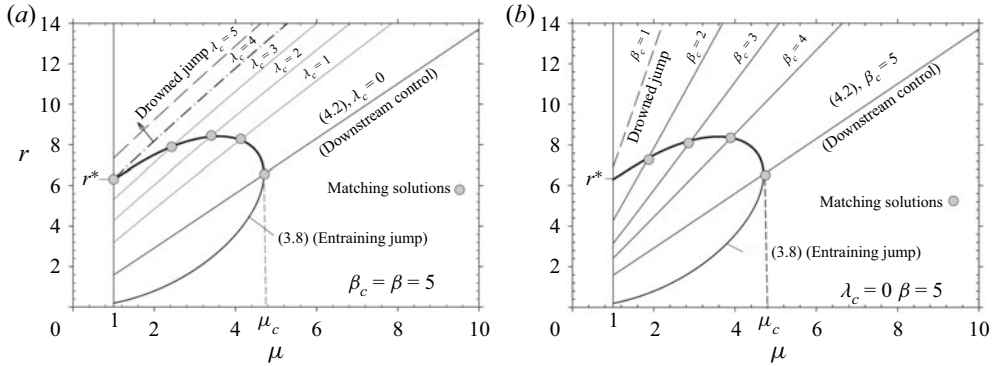
930 A5-12

Figure 11. Matching solutions for overflow jumps obtained by superimposing (4.2) [downstream control] and (3.8) [momentum equation]; $Fr_0 = 10$, $\beta = 5$, $T_a = 20\,°C$, $S_a = 30$ ppt, $\Delta T_0 = +10\,°C$ and $\Delta S_0 = +5$ ppt: (*a*) vertical sill heights λ_c ranging from 0 to 5; and (*b*) horizontal contractions β_c ranging from 1 to 5.

Figure 11(*a*) demonstrates the effect of a vertical sill on an overflow jump. When the relative height of the sill λ_c is increased from 0 to 4, the dilution in the jump region decreases from the maximum dilution $\mu = \mu_c$ for $\lambda_c = 0$ to the minimum dilution $\mu = 1$ for $\lambda_c = 4$. In figure 11(*a*), when $\lambda_c > 4$, (4.2) does not intersect (3.8). Such condition (e.g. $\lambda_c = 5$ in figure 11*a*) indicates that there is no *free* entraining jump solution. In this case, (4.2) at $\mu = 1$ gives $r > r^*$. In other words, the flow cannot simultaneously satisfy both the discharge and the hydraulic control conditions. As previously documented by Baddour and Abbink (1983), this condition produces the so-called drowned jump. The roller of a drowned jump was observed to move all the way upstream and submerge the exit. Entrainment in drowned jumps is suppressed and dilution $\mu \sim 1$ (Baddour 1987).

A similar behaviour is observed in figure 11(*b*), which shows the effect of a downstream horizontal contraction on the jump solutions. As expected, in the absence of a channel contraction ($\beta_c = \beta = 5$), the dilution in the jump region is maximized and $\mu = \mu_c$. And, as the downstream control width decreases ($\beta c < 5$), the dilution is gradually reduced. Eventually, at some contraction ($\beta_c \sim 1$ in figure 11*b*), entrainment is suppressed and the jump becomes drowned.

Controlling dilution in stratified mixing channels is of practical interest. This work demonstrates how to control dilution in a channel by balancing the effects of upstream and downstream conditions.

5. Comparison with experiment

Guo (1992) carried out a series of 54 overflow internal jump tests in the laboratory using two channels, namely channel A and channel B. Channel A, which was reported in an earlier study by Baddour (1991), was 0.15 m wide, 2.5 m long and 0.35 m deep. In channel A, the dilution in the jump region could be controlled and measured directly with a flowmeter and indirectly obtained from temperature measurements. Both methods provided consistent results. Channel B was assembled inside a 1 m wide flume to simulate conditions in a stratified mixing channel connected to a larger body of water. Channel B had two setups, 0.2 m or 0.4 m wide, and 3 m long and 0.23 m deep. The dilution in the jump region in channel B was obtained from detailed temperature profiles. In channel A and channel B, temperature data were gathered with vertical and horizontal banks of 0.12 mm diameter type T thermocouples connected to a PC data acquisition system.

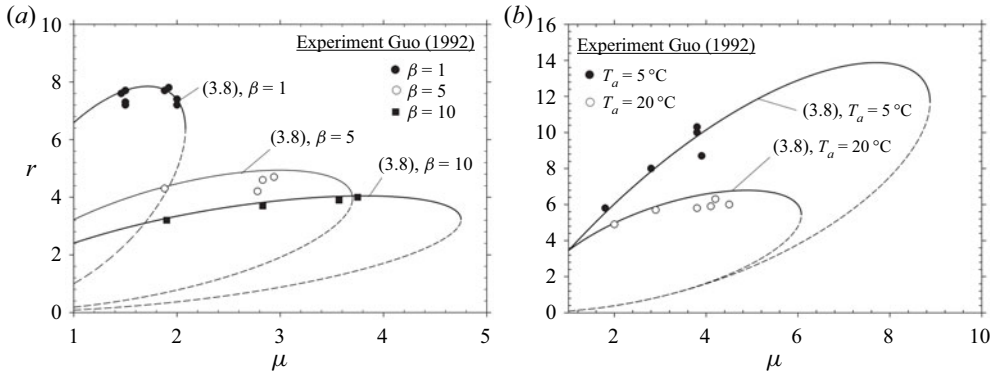| Discharge Froude number, Fr_0	Discharge Reynolds number, Re_0	Channel enlargement ratio, β	Ambient water temperature, T_a (°C)	Discharge excess temperature, ΔT_0 (°C)
5–10	4000–18 000	1–10	5–20	15

Table 1. Testing conditions of 2-D and 3-D experiments by Guo (1992).

Figure 12. Comparison of theory with the experiment by Guo (1992): (*a*) $Fr_0 = 5$, $T_a = 20$ °C, $\Delta T_0 = 15$ °C; (*b*) $Fr_0 = 7.5$, $\beta = 10$, $\Delta T_0 = 15$ °C.

The response time of the thermocouples was 0.01 s. The data acquisition system was programmed to simultaneously scan, at a frequency of 10 Hz, the output of up to 15 probes for a period of 100 s. The conditions of the tests by Guo (1992) are summarized in table 1.

For channel enlargement ratios β between 1 and 10, the horizontal temperature profiles downstream of the jump were practically uniform across the width of the channel. For higher values of β, the horizontal profiles were expected to gradually become non-uniform and eventually Gaussian in shape when β was very large. For such wide channel enlargement ratios, appropriate profile shape parameters would have to be incorporated in the formulation of (3.8) and (4.2).

The experimental data of Guo (1992) are compared in Figures 12 and 13 with the theory developed in this paper. There was generally good agreement between theory and experiment in the entire range of testing conditions. In particular, figure 12(*b*) confirms the predicted effects of nonlinear mixing. The experiments by Guo (1992) did not include salinity variations. To the author's best knowledge, detailed experimental data on stationary entraining jumps with buoyancy produced by differences in temperature and salinity, have not yet been published.

6. Concluding remarks

The nonlinear buoyancy of stationary thermohaline jumps was investigated in this study with a function derived from a nonlinear seawater equation of state. The proposed buoyancy function was obtained with a polynomial transformation and was accurate throughout the range of temperature and salinity of interest ($T = 0$–40 °C and $S = 0$–40 ppt) and can be applied in modelling flows in the ocean and inland waters.
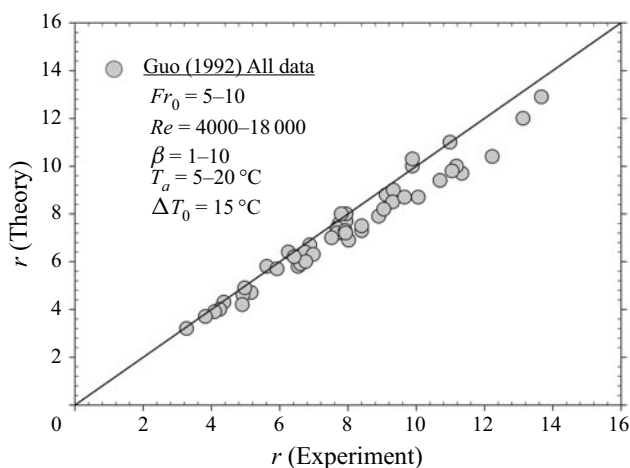
930 A5-14

Figure 13. Comparison of theory with all 2-D and 3-D experiments by Guo (1992).

Nonlinear buoyancy effects were found to be significant when buoyancy arising from temperature and that from salt were acting in opposite directions. Thermohaline overflow jumps achieved greater depths and were capable of entraining more ambient fluid than linear saline jumps. However, thermohaline underflow jumps were shallower and less diluted than linear saline jumps. A matching technique was applied to determine the effect of a downstream control on the miscible jump solution.

Two-dimensional and three-dimensional overflow jump experiments by Guo (1992) are in good agreement with the nonlinear jump theory presented in this paper. Nevertheless, further nonlinear mixing experiments designed specifically to examine the combined buoyancy effects of temperature and salinity on the development of stationary overflow and underflow jumps have not yet been published and are highly recommended.

Finally, it is also recommended to incorporate nonlinear buoyancy equations in the models of oceanic internal hydraulic jumps.

Declaration of interest. The author reports no conflict of interest.

Author ORCIDs.
Raouf Emile Baddour http://orcid.org/0000-0002-9024-3537.

REFERENCES

ARMI, L. 1986 The hydraulics of two flowing layers with different densities. *J. Fluid Mech.* **163**, 27–58.
ARMI, L. & FARMER, D.M. 1988 The flow of Mediterranean water through the Strait of Gibraltar. *Prog. Oceanogr.* **21**, 1–105.
BADDOUR, R.E. 1987 Hydraulics of shallow and stratified mixing channel. *J. Hydraul. Engng* **113**, 630–645.
BADDOUR, R.E. 1991 Thermal hydraulic jump: theory and experiment. *J. Fluid Mech.* **226**, 243–256.
BADDOUR, R.E. 1994 Thermal-saline bubble plumes. In *Recent Advances in the Fluid Mechanics of Turbulent Jets and Plumes*, pp. 117–129. Kluwer Academic.
BADDOUR, R.E. & ABBINK, H. 1983 Turbulent underflow in a short channel of limited depth. *J. Hydraul. Engng* **109** (5), 722–740.

BAINES, P.G. 1984 Unified description of two-layer flow over topography. *J. Fluid Mech.* **146**, 127–167.

BAINES, P.G. 1998 *Topographic Effects in Stratified Flows*. Cambridge University Press.

BAINES, P.G. 2016 Internal hydraulic jumps in two-layer systems. *J. Fluid Mech.* **787**, 1–15.

BENTON, G.S. 1954 The occurrence of critical flow and hydraulic jumps in a multi-layered fluid system. *J. Meteorol.* **11**, 139–150.

BIGG, P.H. 1967 Density of water in SI units over the range 0–40C. *Brit. J. Appl. Phys.* **18**, 521–525.

BRYDON, D., SUN, S. & BLECK, R. 1999 A new approximation of the equation of state for seawater, suitable for numerical ocean models. *J. Geophys. Res.* **104** (C1), 1537–1540.

CHU, V.H. & BADDOUR, R.E. 1977 Surges, waves and mixing in a two-layer density stratified flow. In *Proceedings of the XVIIth Congress*, pp. 303–310. IAHR.

DADONAU, M., PARTRIDGE, J.L. & LINDEN, P.F. 2020 The effect of double diffusion on the dynamics of horizontal turbulent thermohaline jets. *J. Fluid Mech.* **905** (A23), 1–20.

GUO, L.-L. 1992 Internal jumps in stratified cooling channels. MESc thesis, University of Western Ontario, London, Canada.

HASSID, S., REGEV, A. & POREH, M. 2007 Turbulent energy dissipation in density jumps. *J. Fluid Mech.* **572**, 1–12.

HENDERSON, F.M. 1966 *Open Channel Flow*. Macmillan Publishing Company.

HOLLAND, D.M., ROSALES, R.R., STEFANICA, D. & TABAK, E.G. 2002 Internal hydraulic jumps and mixing in two-layer flows. *J. Fluid Mech.* **470**, 63–83.

LAWRENCE, G.A. 1993 The hydraulics of steady two-layer flow over a fixed obstacle. *J. Fluid Mech.* **254**, 605–633.

LONG, R.R. 1953 Some aspects of the flow of stratified fluid I. A theoretical investigation. *Tellus* **5**, 42–58.

LONG, R.R. 1954 Some aspects of the flow of stratified fluid II. Experiments with a two-fluid system. *Tellus* **6**, 97–115.

MILLERO, F.J. 2010 History of the equation of state of seawater. *Oceanography* **23**, 19–33.

MILLERO, F.J. & POISSON, A. 1981 International one-atmosphere equation of state of seawater. *Deep Sea Res.* **28A**, 625–629.

NYCANDER, J., HIERONYMUS, M. & ROQUET, F. 2015 The nonlinear equation of state of seawater and the global water mass distribution. *Geophys. Res. Lett.* **42**, 1–8.

OGDEN, K.A. & HELFRICH, K.R. 2016 Internal hydraulic jumps in two-layer flows with upstream shear. *J. Fluid Mech.* **789**, 64–92.

ROUSE, H. 1946 *Elementary Mechanics of Fluids*. Dover Publications.

STOMMEL, H. & FARMER, H.G. 1953 Control of salinity in an estuary by a transition. *J. Mar. Res.* **12** (1), 13–20.

THORPE, S.A. & LI, L. 2014 Turbulent hydraulic jumps in a stratified shear flow. *J. Fluid Mech.* **758**, 94–120.

THORPE, S.A., MALARKEY, J., VOET, G., ALFORD, M.H., GIRTON, J.B. & CARTER, G.S. 2018 Application of a model of internal hydraulic jumps. *J. Fluid Mech.* **834**, 125–148.

TURNER, J.S. 1966 Jets and plumes with negative or reversing buoyancy. *J. Fluid Mech.* **26**, 779–792.

WHITEHEAD, J.A. 1995 Thermohaline ocean processes and models. *Annu. Rev. Fluid Mech.* **27**, 89–113.

WILKINSON, D.L. & WOOD, I.R. 1971 A rapidly varied flow phenomenon in a two-layer flow. *J. Fluid Mech.* **47**, 241–256.

WOOD, I.R. & SIMPSON, J.E. 1984 Jumps in layered miscible fluids. *J. Fluid Mech.* **140**, 329–342.

YIH, C.-S. & GUHA, C.R. 1955 Hydraulic jump in a fluid system of two layers. *Tellus* **7**, 358–366.